Grazing Incidence X-ray Diffraction Studies of Lipid–Peptide Mixed Monolayers during Shear Flow

Pradip Bera, Ajoy Kandar, Rema Krishnaswamy, Philippe Fontaine, Marianne Impéror-Clerc, Brigitte Pansu, Doru Constantin, Santanu Maiti, Milan Sanyal, A. Sood

ACS OMEGA

http://pubs.acs.org/journal/acsodf

Article

Grazing Incidence X-ray Diffraction Studies of Lipid−Peptide Mixed Monolayers during Shear Flow

Pradip K. Bera, Ajoy K. Kandar, Rema Krishnaswamy, Philippe Fontaine, Marianne Impéror-Clerc, Brigitte Pansu, Doru Constantin, Santanu Maiti, Milan K. Sanyal, and A. K. Sood*

Cite This: *ACS Omega* 2020, 5, 14555−14563

Read Online

ACCESS | Metrics & More | Article Recommendations | Supporting Information

ABSTRACT: Grazing incidence X-ray diffraction (GIXD) studies of monolayers of biomolecules at an air−water interface give quantitative information of in-plane packing, coherence length of crystalline domains, etc. Rheo-GIXD measurements can reveal quantitative changes in the nanocrystalline domains of a monolayer under shear. Here, we report GIXD studies of monolayers of alamethicin peptide, DPPC lipid, and their mixtures at an air−water interface under steady shear stress. The alamethicin monolayer and the mixed monolayer show a flow jamming transition. On the other hand, the pure 1,2-dipalmitoyl-*sn*-glycero-3-phosphocholine (DPPC) monolayer under constant stress flows steadily with a notable enhancement of the area/molecule and coherence lengths, suggesting the fusion of nanocrystallites during flow. The DPPC−alamethicin mixed monolayer shows no significant change in the area/DPPC molecule, but the coherence lengths of the individual phases (DPPC and alamethicin) increase, suggesting that the crystallites of individual phases grow bigger by merging of domains. More phase separation occurs in the system during flow. Our results show that rheo-GIXD has the potential to explore in situ molecular structural changes under rheological conditions for a diverse range of confined biomolecules at interfaces.

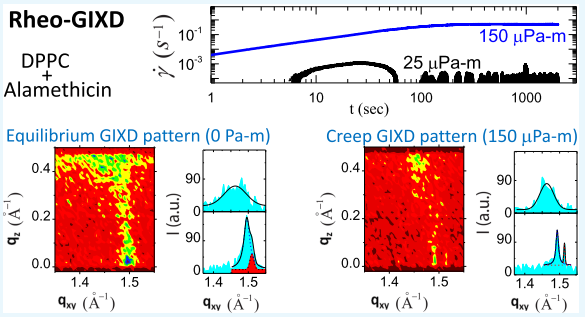

INTRODUCTION

A Langmuir monolayer, a molecularly thin film of amphiphilic molecules stabilized at a liquid−air interface, is an important model system for studying self-organized biological structures, such as cell membranes and lung alveoli, and also has important industrial applications, such as in foam, emulsions, etc.[1−4] A combination of grazing incidence X-ray diffraction (GIXD), specular X-ray reflectivity (XR), and, more recently, electrochemical scanning tunneling microscopy (EC-STM) of Langmuir−Blodgett (LB) monolayers has been used to understand different kinds of phase transitions, molecular structures within crystalline domains (crystallites), and formation of single layers and bilayers.[5−9] Mixed systems such as lipid−cholesterol and lipid−peptide monolayers have been studied to probe the interactions of lipids with other molecules and their relative orientation.[10−15]

Alamethicin is an antimicrobial peptide, produced by many living organisms to defend against Gram-negative and Gram-positive bacteria, fungi, enveloped viruses, eukaryotic parasites, and even tumor cells. Alamethicin isolated from *Trichoderma viride* has 20 residue peptides with a predominantly α-helical structure. In the helical conformation, the length of the molecule is 33 Å. The helix oriented parallel to the interface is called the surface (S) state. If it is inserted into the lipid matrix with the helical axis perpendicular to the interface, it is called the inserted (I) state. The aggregation properties and flow behavior of alamethicin in the form of a Langmuir monolayer were studied using fluorescence microscopy and surface rheology.[16] Fluorescence microscopy showed the coexistence of liquid-expanded and solid phases. The net area fraction of the solid phase increased with concentration. Interfacial rheology showed that the peptide monolayer at a concentration of 800 Å^2/molecule and above had yield stress, which increased with surface concentration.

Biological lipid rafts are dynamic self-organized membrane microdomains that can recruit specific peptides and lipids selectively, while excluding others.[17] The lipid 1,2-dipalmitoyl-*sn*-glycero-3-phosphocholine (DPPC) shows a variety of different ordered states due to the steric and van der Waals interactions between neighboring head groups and alkyl chains. DPPC monolayers exhibit a disordered liquid-expanded (LE) phase that transforms into a liquid-condensed (LC) phase with long-range orientational and short-range positional order at high concentrations. The DPPC monolayer was studied using in situ fluorescence microscopy to correlate

Received: March 21, 2020
Accepted: April 10, 2020
Published: June 9, 2020

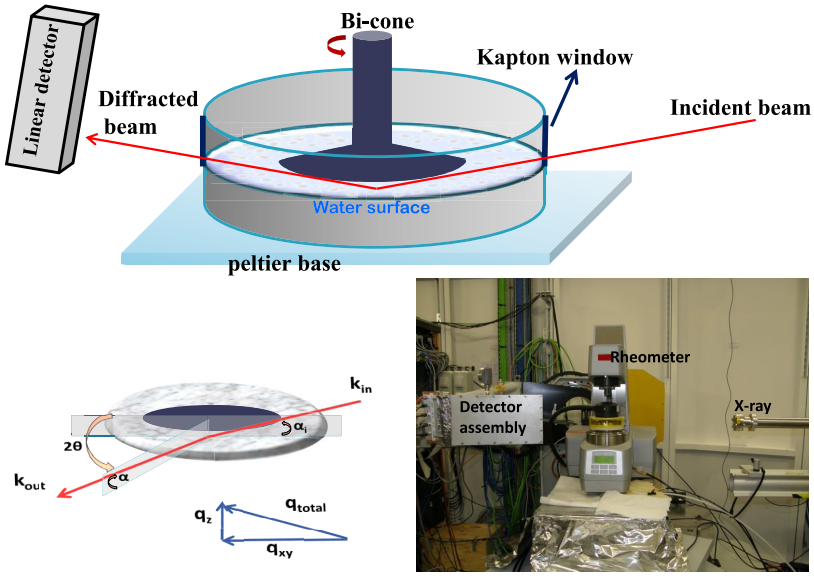

Figure 1. Schematic of the in situ rheo-GIXD setup, showing the water-filled IRS cell on the rheometer's Peltier base, the position of the bi-cone on the interface, and the path of the X-ray beam through the Kapton window striking the annular-shaped interface (top). (Bottom left) schematic of the GIXD mechanism: the vertical incidence angle (α_i), the horizontal scattering angle (2θ), and the vertical exit angle (α); in-plane wave vector $q_{xy} \simeq (4\pi/\lambda) \sin(2\theta/2)$ and out-of-plane wave vector $q_z = (2\pi/\lambda)(\sin\alpha + \sin\alpha_i)$ are shown. (Bottom right) photograph of the experimental setup showing the X-ray source, the rheometer on a z-stage, and the detector assembly attached to the goniometer.

domain dynamics with shear flow.[18−21] In the high-concentration limit, the thin domain boundaries were only visible by fluorescence and it was proposed that the interlocked domains gave rise to the yield stress response of the liquid-condensed-DPPC (LC-DPPC) monolayer. The domain topology was preserved for small shear rates. The lipid interaction with peptides and their structural organization are governed by electrostatic and hydrophobic interactions. Recently, molecular imaging techniques, such as STM, surface-enhanced infrared absorption (SEIRA) spectroscopy, etc., have revealed hexameric pore formation in lipid membranes.[22,23] Even though in situ GIXD has been proposed as a potential probe to monitor the dynamic structure of the crystallites of model membranes,[3,20] there has been no molecular-level structural study of model membranes at an air−water interface under shear force so far.

In this work, we present in situ GIXD along with interfacial rheology to understand changes in the membrane lattice structure under nonequilibrium steady-state flow conditions. Rheo-GIXD measurements are done on three model systems: alamethicin, DPPC, and DPPC−alamethicin mixed monolayers, at different applied stress values.

EXPERIMENTAL DETAILS

Materials. The lipid with two hydrocarbon chains, 1,2-dipalmitoyl-*sn*-glycero-3-phosphocholine (DPPC), and the peptide, alamethicin (all from M/s Avanti Polar Lipids, Inc.), were used without further purification. A mixture of chloroform and methanol (1:1 v/v) was used as a volatile solvent to dissolve the peptide and lipid molecules. The required amount of the solution was spread on the air−water interface using a microsyringe (M/s Hamilton, 50 μL) to obtain an annular-shaped interfacial layer between the bi-cone and the co-centric homemade shear cell, after the evaporation of the solvent.[16] A deionized water subphase (M/s Millipore, with a resistivity of 18.2 MΩ·cm) was used for the DPPC monolayer. For pure alamethicin and DPPC−alamethicin (molar ratio [alamethicin]/[DPPC] = 1:2) mixed monolayers, the subphase was an aqueous solution of 0.1 mole NaCl (pH 7), which was adjusted with 10^{-3} mole phosphate buffer (Na_2HPO_4/NaH_2PO_4 1:1, M/s Merck).

Rheo-GIXD Measurements. The rheo-GIXD experiments were carried out at the SIRIUS beamline of the SOLEIL Synchrotron, France, using an X-ray photon energy of 8 keV ($\lambda \approx 1.55$ Å) at 285 K.[24] This low value of temperature is chosen to minimize the evaporation of water, which could change the bi-cone coupling to the interface. A stress-controlled rheometer (M/s Anton Paar, model MCR-501) fitted with a homemade interfacial shear cell (radius = 65 mm) based on the bi-cone geometry (radius = 34.14 mm) was mounted on the SIRIUS beamline. A schematic of the experimental setup is shown in Figure 1. The dimension of the X-ray beam footprint on the liquid surface was maintained to be ∼1.5 × 20 mm^2 (velocity gradient−velocity direction) by the slits attached to the X-ray source. As the X-ray grazing angle was very small, the shear cell was slightly overfilled to get a just inverted meniscus. The position of the rheometer was set to have the X-ray beam ∼5 mm away from the cone edge. After each loading, to make the X-ray footprint strike at the same position on the surface, the height of the motorized stage was adjusted to bring the liquid surface to the desired height by scanning the specular reflection of the X-ray. The local velocity of the region scanned was $\approx \dot{\gamma} \times y$ (here, $\dot{\gamma}$ is the global shear rate in the system and y = 25 mm is the distance of the X-ray footprint from the cell wall). Water-saturated helium was injected slowly inside the cell from the top to reduce scattering from the air. The monochromatic X-ray beam was adjusted to strike the interface at an incident angle α_i = 2.28 mrad, which corresponded to 0.85 α_c, where α_c is the critical angle of the air−water interface[1] corresponding to the wavelength. A linear (one-dimensional (1D)) gas-filled position-sensitive detector (PSD) fitted with a goniometer was used to record the diffraction pattern by varying the horizontal

https://dx.doi.org/10.1021/acsomega.0c01261
ACS Omega 2020, 5, 14555−14563

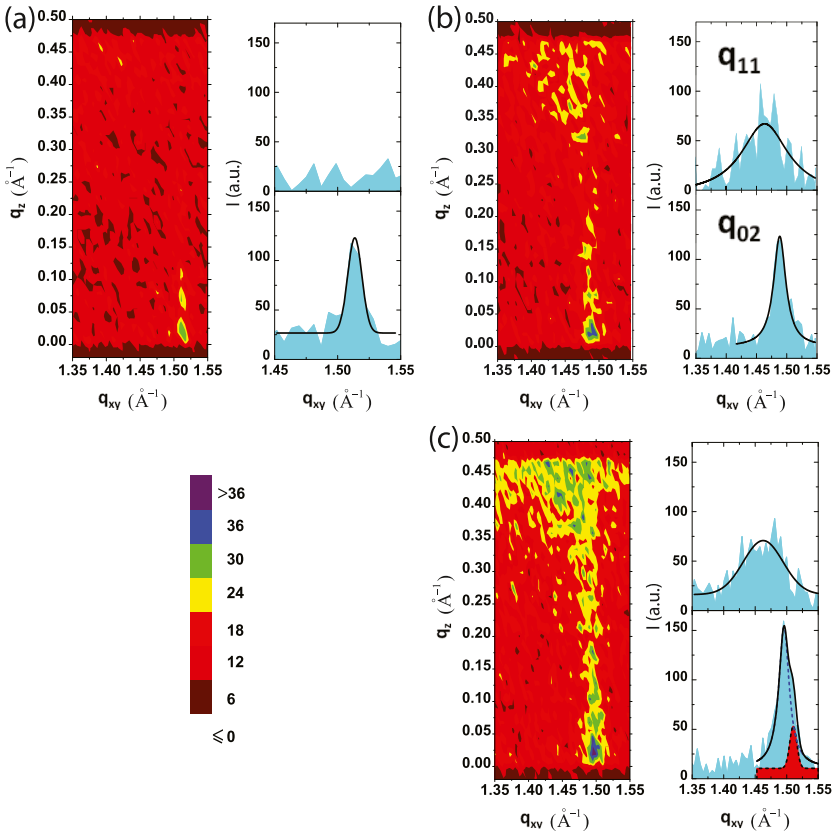

Figure 2. GIXD intensity contours in the (q_{xy}, q_z) plane and Bragg peaks (I vs q_{xy}) of the three monolayers, (a) alamethicin, (b) DPPC, and (c) DPPC−alamethicin, are shown under no-shear conditions at 285 K. Solid lines are fits using a Voigt function. In (c), for the bottom Bragg peak, the solid line is the resultant fit with two peaks (blue dotted line and red shaded black dotted line). Color bars represent intensity values in contours.

angle 2θ from low to high. Soller slits with an angular resolution of 0.02° were used.

After spreading the sample solution at 300 K, the cell was covered with a Teflon cover and then left for 2000 s to let the spreading solvent evaporate under a slow helium flow. During this process, an oscillatory shear of strain amplitude $\gamma_0 = 0.001$ with an angular frequency $\omega = 10$ rad/s was applied to follow up the formation of the monolayer. To maintain identical initial conditions before each creep measurement, monolayers were presheared at $\sigma = 250$ μPa·m for 200 s, and then the system was allowed to equilibrate for 300 s. After 500 s from the starting of creep measurements, GIXD measurements were started to scan the system in the steady flow state.

GIXD Data Analysis. Two-dimensional (2D) diffraction plots for all three monolayers at rest are shown in Figure 2. As a check, a smooth background is observed in GIXD plots from the clean water surface without any feature. The in-plane scattering wave vector, q_{xy}, gives information about the Bragg peaks in the velocity−velocity gradient plane ($V \times \nabla V$). On the other hand, the out-of-plane scattering wave vector, q_z, gives information about the Bragg rods.[1,14] q_{xy} and q_z are expressed in terms of the vertical incidence angle (α_i), horizontal scattering angle (2θ), and vertical exit angle (α) as[6]

$$\frac{q_{xy}}{k} = \sqrt{(\cos\alpha - \cos\alpha_i)^2 + 2\cos\alpha\cos\alpha_i(1 - \cos 2\theta)}$$
$$\simeq \sqrt{(1 + \cos\alpha^2 - 2\cos\alpha\cos 2\theta)}$$
$$\simeq 2\sin(2\theta/2) + O(\alpha^2) \quad (1)$$

$$\frac{q_z}{k} = \sin\alpha + \sin\alpha_i \quad (2)$$

where $k = 2\pi/\lambda$ and $\cos\alpha_i \approx 1$ for a very small value of α_i.

The observed peaks are well separated in the $q_{xy} - q_z$ contour plots. We note small differences with respect to the monolayers prepared in the LB trough,[10,12,14] arising because our experiments are done on a spread monolayer, instead of compressing it from a liquid-expanded phase, and later, it is in the flow state. It has been shown that the quantitative deviation of the oblique unit cell from the 2D centered rectangular unit cell is small.[1] The oblique unit cell of enantiomeric DPPC has been reported in recent studies with monolayers compressed from a very low surface concentration. However, here, the splitting of the peak at a high q_z value is not observed, maybe due to the fact that we have highly concentrated spread monolayers and also due to the boundary curvature arising from the presence of the bi-cone. Thus, we assume the rectangular unit cell model, which is sufficient for the present work. We have adopted the box integration method for each peak, as discussed below. The Bragg peaks are observed by integrating the contours from q_z

https://dx.doi.org/10.1021/acsomega.0c01261
ACS Omega 2020, 5, 14555−14563

Table 1. Structural Packing Parameters of the DPPC Monolayer for Different σ Values

σ [μPa·m]	d-spacings [Å]	unit cell dimensions [Å]	$A_{molecule}$ [Å^2]	coherence length [Å]
0	d_{11} = 4.293 ± 0.015	a = 4.986 ± 0.024	42.09 ± 0.23	L_{11} = 76 ± 7
	d_{02} = 4.221 ± 0.003	b = 8.443 ± 0.006		L_{02} = 256 ± 15
10	d_{11} = 4.328 ± 0.010	a = 5.042 ± 0.017	42.54 ± 0.16	L_{11} = 69 ± 5
	d_{02} = 4.218 ± 0.002	b = 8.437 ± 0.004		L_{02} = 314 ± 40
20	d_{11} = 4.350 ± 0.009	a = 5.072 ± 0.015	42.90 ± 0.15	L_{11} = 83 ± 6
	d_{02} = 4.229 ± 0.002	b = 8.459 ± 0.005		L_{02} = 627 ± 103
50	d_{11} = 4.384 ± 0.012	a = 5.123 ± 0.020	43.40 ± 0.19	L_{11} = 74 ± 6
	d_{02} = 4.236 ± 0.002	b = 8.472 ± 0.004		L_{02} = 620 ± 55
100	d_{11} = 4.359 ± 0.005	a = 5.088 ± 0.008	43.02 ± 0.08	L_{11} = 106 ± 5
	d_{02} = 4.227 ± 0.002	b = 8.455 ± 0.003		L_{02} = 447 ± 29

Table 2. Structural Packing Parameters of the DPPC−Alamethicin Mixed Monolayer for Different σ Values

σ [μPa·m]	DPPC d-spacings, alamethicin pitch [Å]	DPPC unit cell dimensions [Å]	DPPC $A_{molecule}$ [Å^2]	coherence length [Å]; DPPC L_{hk}, alamethicin Lp
0	d_{11} = 4.296 ± 0.009	a = 4.999 ± 0.016	42.00 ± 0.16	L_{11} = 85 ± 6
	d_{02} = 4.201 ± 0.003	b = 8.402 ± 0.005		L_{02} = 314 ± 17
	p = 4.160 ± 0.005			L_p = 396 ± 96
25	d_{11} = 4.294 ± 0.005	a = 4.993 ± 0.008	42.02 ± 0.10	L_{11} = 134 ± 8
	d_{02} = 4.208 ± 0.003	b = 8.416 ± 0.007		L_{02} = 741 ± 92
	p = 4.150 ± 0.005			L_p = 1510 ± 459
50	d_{11} = 4.284 ± 0.007	a = 4.981 ± 0.012	41.81 ± 0.15	L_{11} = 134 ± 11
	d_{02} = 4.197 ± 0.004	b = 8.395 ± 0.009		L_{02} = 321 ± 36
	p = 4.140 ± 0.003			L_p = 1611 ± 305
75	d_{11} = 4.303 ± 0.005	a = 5.003 ± 0.009	42.20 ± 0.12	L_{11} = 132 ± 8
	d_{02} = 4.218 ± 0.004	b = 8.435 ± 0.008		L_{02} = 413 ± 58
	p = 4.153 ± 0.006			L_p = 1250 ± 355
150	d_{11} = 4.300 ± 0.005	a = 4.999 ± 0.008	42.14 ± 0.07	L_{11} = 120 ± 17
	d_{02} = 4.215 ± 0.001	b = 8.429 ± 0.001		L_{02} = 772 ± 31
	p = 4.151 ± 0.002			L_p = 1050 ± 91

= 0 to 0.1 Å^{-1} and from 0.3 to 0.5 Å^{-1}. The Bragg peaks are fitted with a Voigt function along with the background intensity to get the peak centers and the full width at half-maximum (FWHM).[10] For DPPC, lattice distances $d_{hk} = 2\pi/q_{hk}$ are extracted using the Bragg peaks q_{02} and q_{11} and then fitted to the 2D centered rectangular unit cell model to get the lattice parameters a and b[6,14] and, hence, the area/molecule. With the Scherrer equation, the FWHM values of the Bragg peaks were used to determine the coherence length, L ($L = 2\pi$/FWHM), which can be approximated as the average size of the nanocrystallites. We have restricted our study to $q_{xy} \geq 1.0$ Å^{-1}; below this limit, the noise increases significantly toward the direct beam.

RESULTS AND DISCUSSION

We have calibrated our rheo-GIXD setup using a behenic acid monolayer as a test sample and that validates our GIXD setup (see the Supporting Information Section A). It can be seen that the GIXD pattern in ref 25 (see Figure 1(b) of ref 25) is qualitatively similar to that recorded by us (Figure S1(a)). The pattern in the q_{xy} direction is the same as that in ref 25. There are, however, differences in the q_z direction. The separation between the two peaks is $\Delta q_z \sim 0.55$ Å^{-1} in ref 25 and $\Delta q_z \sim 0.45$ Å^{-1} in our case. Δq_z is related to the molecular tilt of behenic acid. The presence of the bi-cone (Figure S1(b)), however, does make a change in the out-of-plane GIXD peak, primarily due to the boundary curvature arising from the presence of the bi-cone. Due to the irregular shape of the out-of-plane peaks observed in our rheo-GIXD data, we do not calculate the molecular tilt angle. Note that in the earlier GIXD reports with LB films, the GIXD scans were done in the interior region of the films, where the curved boundaries do not affect the molecular tilt. Also, the sensitivity of the monolayers to the small imposed torque on the measuring bi-cone geometry was checked using test monolayers with cholesterol, which is known for showing a very low surface viscosity[26] (see Supporting Information Section B). With the cholesterol and cholesterol mixed monolayers, we get a very high value of the shear rate ($\dot{\gamma}$), which confirms the good sensitivity of the monolayers even to the very small interfacial stress (σ in units of μPa·m) imposed by the rheometer.

Equilibrium Study of Alamethicin, DPPC, and DPPC−Alamethicin Mixed Monolayers. Before applying shear to the monolayers at the annular-shaped air−water interface between the bi-cone and the shear cell, their structural properties were characterized. Figure 2 shows the equilibrium diffraction patterns of alamethicin, DPPC, and DPPC−alamethicin mixed monolayers. The alamethicin monolayer was prepared for 12 Å^2/molecule surface concentration as lower concentrations do not give rise to a measurable diffraction peak in the GIXD pattern. The equilibrium GIXD pattern shows a strong peak at $q_{xy} = 1.514$ Å^{-1} near $q_z = 0$, confirming that the alamethicin molecules are adsorbed on the surface. The observed strong peak due to alamethicin corresponds to the pitch of the helix of 4.15 Å (Figure 4c), which is quite small compared with the pitch of 5.4 Å for a free α-helix. This reduction in helix pitch is due to the compact packing of alamethicin molecules on the water surface at this high concentration, consistent with a previous

https://dx.doi.org/10.1021/acsomega.0c01261
ACS Omega 2020, 5, 14555−14563

study of the helical scattering distribution of alamethicin.[27] The coherence length estimated from the measured line width (~475 Å) suggests that there are domains of at least 14 correlated molecules. The expected hexagonal lattice ordering, forming holes inside these domains,[22] with lattice parameters of a = 19 Å, should show a Bragg peak in the low-q range, which is not seen in our experiments due to the high background intensity near the direct beam, and hence, we cannot estimate the area/molecule from the GIXD data.

The GIXD pattern from DPPC (solution concentration of 0.5 mg/mL) shown in Figure 2b gives area/molecule = 42.1 Å^2. DPPC has a 2D ordering of molecules on the water surface and gives rise to two well-separated Bragg peaks (Figure 2b) at q_{xy} = 1.464 Å^{-1} (q_z = 0.43 Å^{-1}) and q_{xy} = 1.489 Å^{-1} (q_z = 0.03 Å^{-1}). The relative intensity of these two peaks is ~2:1 as expected for the DPPC monolayer.[10] The diffraction pattern is analyzed with the centered rectangular unit cell model of rod-shaped alkyl chains[10] (Table 1). The area/molecule and the coherence lengths are consistent with the values in previous studies.[10]

The DPPC−alamethicin mixed monolayer was prepared with a molar ratio of 1:2 and with surface concentrations of 12 Å^2/alamethicin molecule. The GIXD pattern clearly shows three Bragg peaks (Figure 2c): one is at 1.510 Å^{-1}, representing the alamethicin helix pitch, and the other two are at 1.463 and 1.496 Å^{-1} with 2:1 intensity ratio, associated with the DPPC molecular ordering in the monolayer. The estimated area/molecule of DPPC is 42.0 Å^2, which is very close to that of the pure DPPC monolayer (Table 2). The hexagonal structure of alamethicin in the DPPC−alamethicin[22] mixture could not be observed due to the high direct-beam leakage intensity at low q_{xy}. Note that in equilibrium the alamethicin helix peak is on the shoulder of the DPPC q_{02} Bragg peak, but with shear flow, coherence lengths corresponding to the DPPC q_{02} peak and the alamethicin helix peak increase drastically, and thus, the alamethicin helix peak stands well separated in the GIXD pattern (see Figure 6 and the 2D plots in the TOC).

Stress-Controlled Flow Curve. For the flow curve and other rheological characterization of alamethicin monolayers, see ref 16. Figure 3 shows the stress-controlled flow curves of DPPC and DPPC−alamethicin mixed monolayers. The flow curves of the monolayers are very similar to those of the monolayer in the study by Majumdar et al. (see Figure 3 of ref 28), where the surface deformation profile is studied and the flow inhomogeneity or shear banding is reported in the nonlinear region. To avoid flow inhomogeneity or shear banding, we have chosen the linear flow region as our working region for the two monolayers (as indicated by the blue and black lines with slope ~1). The approximate upper cutoff stress is chosen as the preshear stress (σ = 250 μPa·m) for each creep measurement to erase the history of the system (for details, please see the Experimental Details Section).

Creep Study of the Alamethicin Monolayer. We now proceed to examine the structural changes inside the monolayers in the nonequilibrium steady state under different shear stress conditions. Figure 4a shows the creep behavior of the alamethicin monolayer studied as a function of applied stress up to 50 μPa·m. For all applied stress values (σ), the shear rate ($\dot{\gamma}$) increases linearly with time for ~60 s, showing significant shear rejuvenation in the monolayer before going to the final steady state. The stress values ranging from 2.5 to 50 μPa·m are much above the stress resolution (0.3 μPa·m) of the rheometer. For 2.5 μPa·m ≤ σ ≤ 20 μPa·m, the shear rate is ~10^{-2}−10^{-4} s^{-1} (much higher than the resolution of ~10^{-7} s^{-1}). After ~200 s, the shear rate decreases and fluctuates about zero, though with a positive value of the average shear rate. This observation of shear rate fluctuating about zero is seen in the stress-induced jamming behavior in bulk rheology of a laponite clay suspension.[29] At 50 μPa·m, $\dot{\gamma}$ attains a steady-state value of ~0.06 s^{-1}. Figure 4b shows the GIXD data for the four values of σ, captured during 500−2000 s. The helix peak position remains constant with increasing σ, but the line width shows a variation, reflecting the changes in the domain size (Figure 4c). However, there is no systematic variation of the coherence length with applied stress.

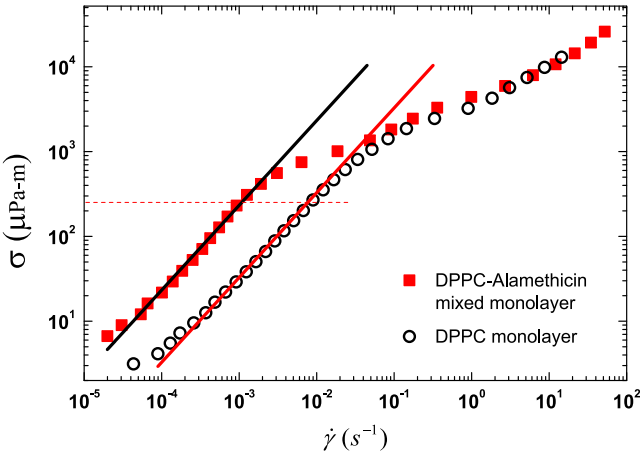

Figure 3. Flow curve, shear stress (σ) vs shear rate ($\dot{\gamma}$), obtained in the controlled shear stress (CSS) mode with a waiting time of 30 s for each data point is shown for the DPPC monolayer and DPPC−alamethicin mixed monolayer at the air−water interface. Solid lines are of slope ~1. The dotted line is the approximate cutoff of the linear flow region (~250 μPa·m).

Creep Study of the DPPC Monolayer. The creep behavior of the DPPC monolayer was studied up to 100 μPa·m (Figure 5). Unlike the alamethicin monolayer, DPPC shows neither substantial shear rejuvenation nor flow jamming. For a given σ, the steady-state shear rate is an order of magnitude lower compared to that of the alamethicin monolayer (50 μPa·m data can be compared). The steady shear viscosity (η) of the DPPC monolayer in our experiments (see Supporting Information Section C) compares very well with the magnitude of the reported complex viscosity[19] ($\eta^*(\omega)$ ~ 2 × 10^{-3} Pa·m·s) at a surface pressure of 45 mN/m (corresponding to an area/molecule of ~40 Å^2). The Bragg peaks, q_{02} and q_{11}, for different σ values are shown in Figure 5b−e. The peak position of q_{02} does not change with stress, whereas the q_{11} peak position shifts to lower values, suggesting elongation of the unit cell under shear flow. Additionally, the width of q_{02} decreases with increasing σ, suggesting the fusion of crystallites during flow. The DPPC crystallite size increases under applied stress. These results are given in Table 1 and are plotted in Figure 8.

Creep Study of the Mixed Monolayer. Figure 6 shows the creep behavior of the DPPC−alamethicin mixed monolayer studied up to 150 μPa·m. Shear rejuvenation is observed with $\dot{\gamma}$ increasing linearly with time. At 25 μPa·m, it shows rejuvenation up to 30 s and then goes to the flow-jammed state after 60 s of flow similar to the pure alamethicin monolayer. At 50 μPa·m and above, it goes to a steady flow

https://dx.doi.org/10.1021/acsomega.0c01261
ACS Omega 2020, 5, 14555−14563

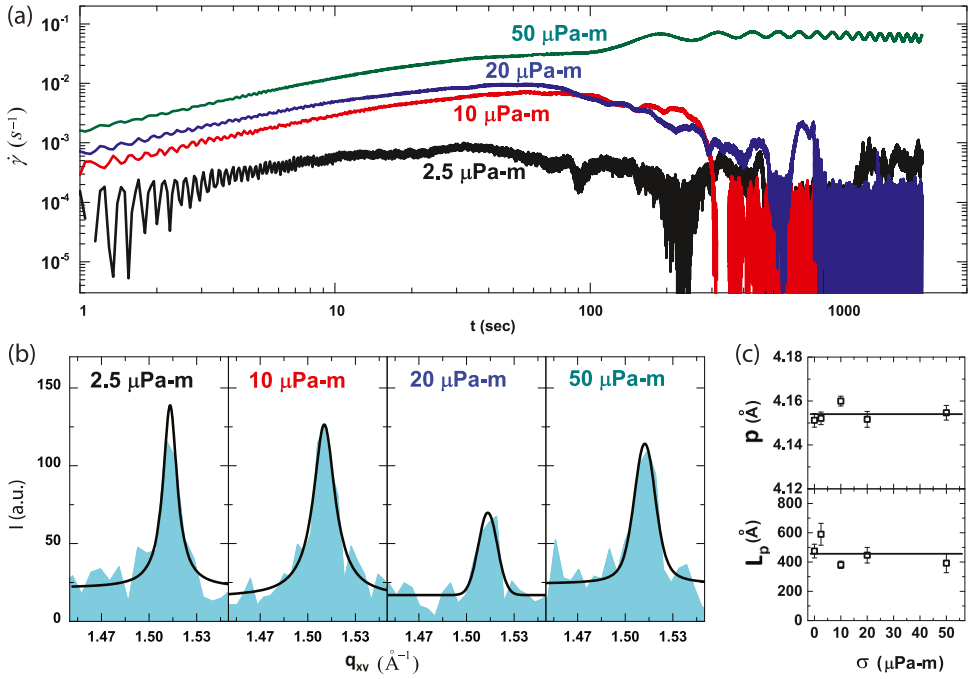

Figure 4. Rheo-GIXD creep data of the alamethicin monolayer (presheared for 200 s followed by a waiting time of 300 s before each measurement; see text): (a) creep curves; shear rate ($\dot{\gamma}$) vs time (t) (applied stress σ is mentioned close to the curves), (b) Bragg peaks (I vs q_{xy}) for different σ values. Solid lines are fits using a Voigt function. The Bragg peak corresponds to the helix pitch of alamethicin. (c) The helix pitch (p) and the coherence length (L_p) are plotted vs σ. Straight horizontal lines represent the average values of p and L_p.

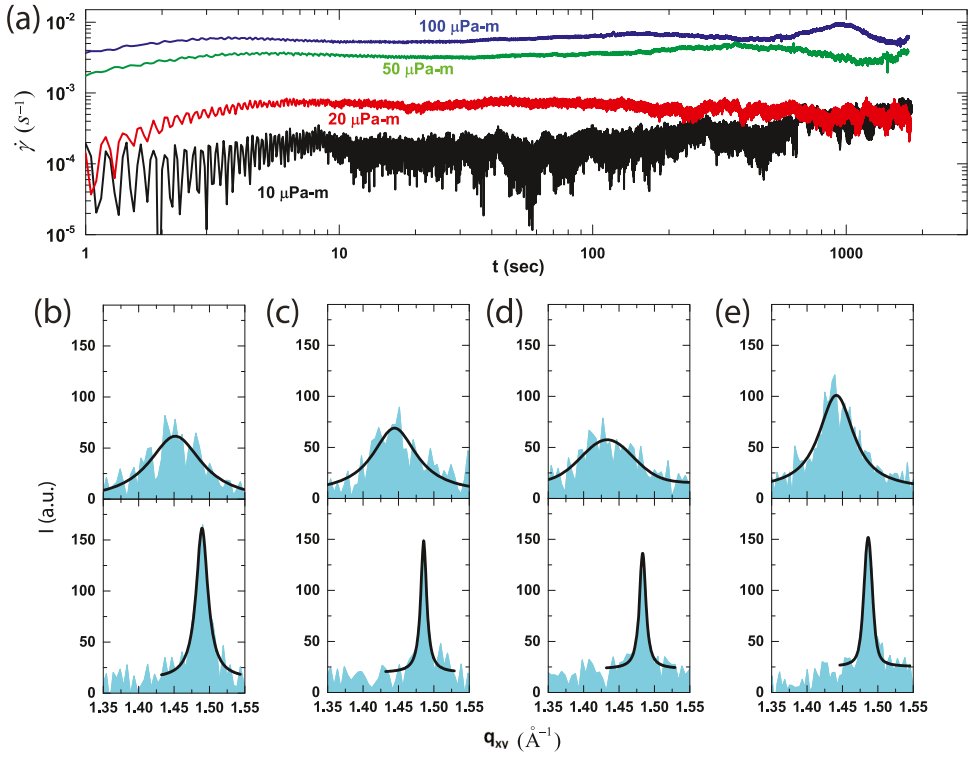

Figure 5. Rheo-GIXD creep data of the DPPC monolayer (presheared for 200 s followed by a waiting time of 300 s before each measurement; see text): (a) creep curves; $\dot{\gamma}$ vs t are plotted. Bragg peaks q_{02} (bottom) and q_{11} (top) for different σ values of (b) 10 μPa·m, (c) 20 μPa·m, (d) 50 μPa·m, (e) and 100 μPa·m are shown. The peaks are fitted using a Voigt function.

state with an enhanced $\dot{\gamma}$ compared to that of the pure alamethicin monolayer, which is orders of magnitude higher compared to that of the pure DPPC monolayer. This suggests that the DPPC crystalline domains are no longer closely packed in the mixed monolayer and stay phase-separated with alamethicin, as evident from the system's high shear rates. Unlike the pure DPPC monolayer, the peak positions of q_{02} and q_{11} do not change during flow (Table 2). Strikingly, the

https://dx.doi.org/10.1021/acsomega.0c01261
ACS Omega 2020, 5, 14555−14563

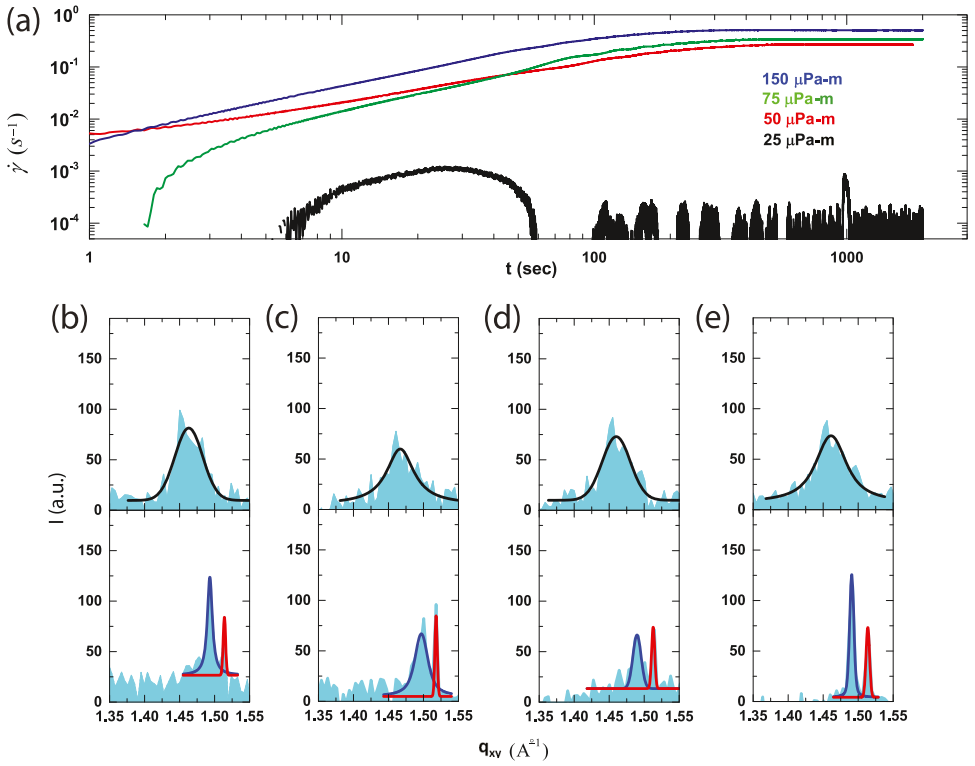

Figure 6. Rheo-GIXD creep data of the DPPC−alamethicin mixed monolayer with the molar ratio P/L = 1:2 (presheared for 200 s followed by a waiting time of 300 s before each measurement; see text): (a) creep curves; $\dot{\gamma}$ vs t are plotted. Bragg peaks q_{02} (blue solid fit) and q_{11} (black solid fit) and the alamethicin helix peak (red solid fit) for different σ values of (b) 25 μPa·m, (c) 50 μPa·m, (d) 75 μPa·m, and (e) 150 μPa·m are shown. The peaks are fitted using a Voigt function.

coherence length of the alamethicin helix increases with σ, suggesting that the alamethicin domains merge to a bigger size promoting more separation of phases in the system.

As noted in ref 6, Langmuir films are 2D powders of randomly oriented 2D crystallites in the plane. Bragg reflections do not capture the motion of the crystallites (whenever the reflecting plane satisfies the Bragg condition, it contributes to the Bragg peak). In a way, the motion of the crystallites in a circular streamline path rather helps us to get the powder diffraction pattern. Effectively, the scan is not at a fixed position on the sample, but rather the pattern is averaged over a large number of crystallites passing through the X-ray footprint.

Figure 7 shows the log−log plot of q_z-integrated intensity vs q_{xy}, which decays linearly and confirms the flatness of the interface[30] during the GIXD measurements. For comparison, we have plotted the area/molecule (A_{molecule}) and coherence lengths (L_{hk}) of DPPC for pure and mixed systems (Figure 8). For the pure DPPC monolayer, the area/molecule (Figure 8a)

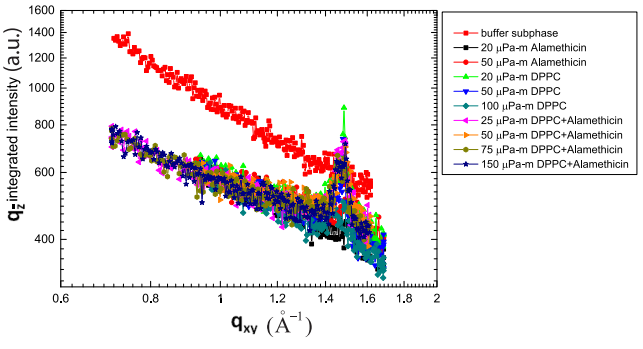

Figure 7. q_z-integrated intensity vs q_{xy} plot for the monolayers during creep flow. The diffraction data from the clean buffer subphase surface are also shown.

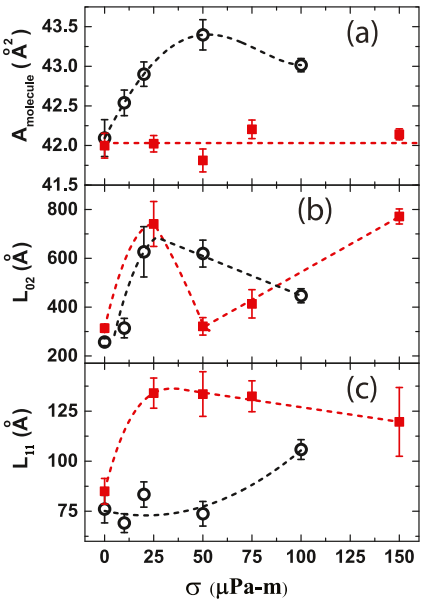

Figure 8. (a) Area/molecule of DPPC (A_{molecule}) and the coherence lengths L_{02} (b) and L_{11} (c) corresponding to the Bragg peaks for pure DPPC (open circles) and DPPC−alamethicin mixed (red squares) monolayers are plotted against σ. Dotted curves are guides to the eyes.

https://dx.doi.org/10.1021/acsomega.0c01261
ACS Omega 2020, 5, 14555−14563

increases rapidly with σ and saturates at high values, whereas for the mixed monolayer, it does not change with σ. For both the systems, the coherence lengths in the [02] direction (L_{02}) increases with increasing shear rate. The data for 25 μPa·m of the mixed monolayer do not follow the trend. We propose that the high value of L_{02} corresponding to 25 μPa·m is due to the flow-merging of crystalline domains during the flow jamming transition. On the other hand, the coherence length in the [11] direction (L_{11}) has a slow increment for the pure DPPC monolayer but shows a high value for the mixed monolayer with increasing shear rate.

CONCLUSIONS

We have described the methodology of rheo-GIXD, an extension of the well-established GIXD technique to study molecular structures under steady shear at an interface by combining interfacial rheology and GIXD. We have demonstrated that the GIXD signal can be captured even when the interfacial molecular crystallites move under shear. At low σ, the pure alamethicin and mixed monolayers show jamming behavior after about ∼100 s. For a given σ, the observed steady-state shear rate for the alamethicin-free system is very high, confirming the finite flow of the system, but the opposite happens for the alamethicin monolayer and the mixed monolayer. Before entering the jammed state, the system flows with a finite shear rate (compare the 20 μPa·m data in Figures 4 and 5), which is sufficiently high to be detected by a commercial rheometer. Thus, we can safely conclude that we have a high signal-to-noise ratio, and this is a genuine flow jamming behavior. The Boussinesq (Bo) number in all our present experiments is much higher than 1 (see Supporting Information Section C). Most importantly, our focus in the present work is not on the extraction of the interfacial viscosity of different monolayers. See refs 31−33 for the subphase contribution to the interfacial viscosity and for a detailed discussion on the interfacial rheology with different geometries. The stress values used in our experiments are in the regime of a linear flow profile, as inferred from our recent experiments on a sorbitan tristearate monolayer.[4] The velocity profile was measured and was shown to be linear up to an applied strain amplitude γ_0 = 0.1, corresponding to a stress amplitude of 0.01 Pa·m (see Figure 1 (b) of ref 4), with Bo∼500.

The pure DPPC monolayer shows measurable changes in lattice parameters. The change in the lattice structure due to shear is interesting and is the focus of the paper, rather than the absolute values. The presence of the buffer subphase stabilizes the peptide at the air−water interface but does not lead to the binding of the peptide with the DPPC head group, as inferred from the observation that the scattering signal is almost similar in both cases (pure DPPC and mixed DPPC−alamethicin). The phase separation and the barrel-stave aggregation of an amphipathic peptide in a peptide−lipid matrix in equilibrium[22] are also consistent with our rheo-GIXD observations under shear. We have shown that the 2D crystallites grow bigger by the merging of crystalline domains under shear. The structural properties of hexameric pores could not be probed here due to high direct-beam leakage in the low-q_{xy} region.

Further work along with X-ray reflectivity studies on this system will allow us to investigate the dependence of structural parameters on the velocity gradient. In the future, the underlying transient dynamics will be probed along with a 1D pinhole detector or with a 2D detector. Also, this technique can be used to probe the molecular dynamics near the nonequilibrium phase transition of monolayers under oscillatory shear deformation.[4] We believe that our results will provide motivation for studying the molecular-level structure of many other membranes under nonequilibrium conditions.

ASSOCIATED CONTENT

Supporting Information

The Supporting Information is available free of charge at https://pubs.acs.org/doi/10.1021/acsomega.0c01261.

Calibration of our rheo-GIXD setup using behenic acid; assessment of the sensitivity of monolayers to the small imposed torque on the measuring bi-cone geometry and calculation of steady shear viscosity; Boussinesq number corresponding to different σ values for different monolayers (PDF)

AUTHOR INFORMATION

Corresponding Author

A. K. Sood − *Department of Physics, Indian Institute of Science, Bangalore 560012, India;* orcid.org/0000-0002-8652-1389; Email: asood@iisc.ac.in

Authors

Pradip K. Bera − *Department of Physics, Indian Institute of Science, Bangalore 560012, India;* orcid.org/0000-0003-0124-4747

Ajoy K. Kandar − *Department of Physics, Indian Institute of Science, Bangalore 560012, India; Soft Condensed Matter, Debye Institute for Nanomaterials Science, Utrecht University, 3584 CC Utrecht, The Netherlands*

Rema Krishnaswamy − *Department of Physics, Indian Institute of Science, Bangalore 560012, India; School of Liberal Studies, Azim Premji University, Bangalore 560100, India*

Philippe Fontaine − *SOLEIL Synchrotron, 91192 Gif-sur-Yvette Cedex, France;* orcid.org/0000-0003-3394-6508

Marianne Impéror-Clerc − *Laboratoire de Physique des Solides, Unité Mixte de Recherche 8502 Centre National de la Recherche Scientifique, Université Paris-Sud 11, 91405 Orsay Cedex, France;* orcid.org/0000-0002-0269-7556

Brigitte Pansu − *Laboratoire de Physique des Solides, Unité Mixte de Recherche 8502 Centre National de la Recherche Scientifique, Université Paris-Sud 11, 91405 Orsay Cedex, France*

Doru Constantin − *Laboratoire de Physique des Solides, Unité Mixte de Recherche 8502 Centre National de la Recherche Scientifique, Université Paris-Sud 11, 91405 Orsay Cedex, France*

Santanu Maiti − *Saha Institute of Nuclear Physics, Kolkata 700064, India*

Milan K. Sanyal − *Saha Institute of Nuclear Physics, Kolkata 700064, India;* orcid.org/0000-0002-3847-8793

Complete contact information is available at: https://pubs.acs.org/10.1021/acsomega.0c01261

Notes

The authors declare no competing financial interest.

ACKNOWLEDGMENTS

A.K.S. thanks the Department of Science and Technology (DST), India, for the support through the Year of Science

Professorship. M.K.S. acknowledges the support through the Raja Ramanna Fellowship of the Department of Atomic Energy (DAE). R.K. thanks DST for the Ramanujan Fellowship. A.K.K. and P.K.B. thank the University Grants Commission (UGC) for the D.S. Kothari Fellowship and Senior Research Fellowship, respectively. We thank DST for financial assistance through the CEFIPRA-SOLEIL-Synchrotron Programme (20140232, AP14/15) to use the synchrotron beamtime. We acknowledge SOLEIL for provision of synchrotron radiation facilities and we thank N. Aubert for assistance in using the beamline SIRIUS. We thank Prof. Jean Daillant for fruitful discussions.

REFERENCES

(1) Als-Nielsen, J.; Jacquemain, D.; Kjaer, K.; Leveiller, F.; Lahav, M.; Leiserowitz, L. Principles and applications of grazing incidence X-ray and neutron scattering from ordered molecular monolayers at the air−water interface. *Phys. Rep.* **1994**, *246*, 251−313.

(2) Kaganer, V. M.; Möhwald, H.; Dutta, P. Structure and phase transitions in Langmuir monolayers. *Rev. Mod. Phys.* **1999**, *71*, 779−819.

(3) Fuller, G. G.; Vermant, J. Complex fluid-fluid interfaces: rheology and structure. *Annu. Rev. Chem. Biomol. Eng.* **2012**, *3*, 519−543.

(4) Bera, P. K.; Kandar, A. K.; Krishnaswamy, R.; Sood, A. K. Experimental signatures of a nonequilibrium phase transition near the crossover point of a Langmuir monolayer. *J. Phys. Condens. Matter* **2019**, *31*, No. 504004.

(5) Kjaer, K.; Als-Nielsen, J.; Helm, C. A.; Laxhuber, L. A.; Möhwald, H. Ordering in lipid monolayers studied by synchrotron X-ray diffraction and fluorescence microscopy. *Phys. Rev. Lett.* **1987**, *58*, 2224−2227.

(6) Kjaer, K. Some simple ideas on X-ray reflection and grazing-incidence diffraction from thin surfactant films. *Phys. B* **1994**, *198*, 100−109.

(7) Miller, C. E.; Majewski, J.; Watkins, E. B.; Mulder, D. J.; Gog, T.; Kuhl, T. L. Probing the local order of single phospholipid membranes using grazing incidence X-ray diffraction. *Phys. Rev. Lett.* **2008**, *100*, No. 058103.

(8) Maiti, S.; Sanyal, M. K.; Mukhopadhyay, M. K.; Singh, A.; Mukherjee, S.; Datta, A.; Fontaine, P. Structural and optical properties of two-dimensional gadolinium stearate Langmuir monolayer. *Chem. Phys. Lett.* **2018**, *712*, 177−183.

(9) Maiti, S.; Maiti, S.; Maier, A.; Hagenlocher, J.; Chumakov, A.; Schreiber, F.; Scheele, M. Understanding the Formation of Conductive Mesocrystalline Superlattices with Cubic PbS Nanocrystals at the Liquid/Air Interface. *J. Phys. Chem. C* **2019**, *123*, 1519−1526.

(10) Watkins, E. B.; Miller, C. E.; Mulder, D. J.; Kuhl, T. L.; Majewski, J. Structure and orientational texture of self-organizing lipid bilayers. *Phys. Rev. Lett.* **2009**, *102*, No. 238101.

(11) Wu, G.; Majewski, J.; Ege, C.; Kjaer, K.; Weygand, M. J.; Lee, K. Y. C. Interaction between lipid monolayers and poloxamer 188: an X-ray reflectivity and diffraction study. *Biophys. J.* **2005**, *89*, 3159−3173.

(12) Neville, F.; Ishitsuka, Y.; Hodges, C. S.; Konovalov, O.; Waring, A. J.; Lehrer, R.; Lee, K. Y. C.; Gidalevitz, D. Protegrin interaction with lipid monolayers: grazing incidence X-ray diffraction and X-ray reflectivity study. *Soft Matter* **2008**, *4*, 1665−1674.

(13) Ivankin, A.; Kuzmenko, I.; Gidalevitz, D. Cholesterol-phospholipid interactions: new insights from surface X-ray scattering data. *Phys. Rev. Lett.* **2010**, *104*, No. 108101.

(14) Watkins, E. B.; Miller, C. E.; Majewski, J.; Kuhl, T. L. Membrane texture induced by specific protein binding and receptor clustering: active roles for lipids in cellular function. *Proc. Natl. Acad. Sci. U.S.A.* **2011**, *108*, 6975−6980.

(15) Broniatowski, M.; Sobolewska, K.; Flasiński, M.; Wydro, P. Studies on the interactions of bisphenols with anionic phospholipids of decomposer membranes in model systems. *Biochim. Biophys. Acta* **2016**, *1858*, 756−766.

(16) Krishnaswamy, R.; Rathee, V.; Sood, A. K. Aggregation of a Peptide Antibiotic Alamethicin at the Air−Water Interface and Its Influence on the Viscoelasticity of Phospholipid Monolayers. *Langmuir* **2008**, *24*, 11770−11777.

(17) Edidin, M. The state of lipid rafts: from model membranes to cells. *Annu. Rev. Biophys. Biomol. Struct.* **2003**, *32*, 257−283.

(18) Espinosa, G.; López-Montero, I.; Monroy, F.; Langevin, D. Shear rheology of lipid monolayers and insights on membrane fluidity. *Proc. Natl. Acad. Sci. U.S.A.* **2011**, *108*, 6008−6013.

(19) Hermans, E.; Vermant, J. Interfacial shear rheology of DPPC under physiologically relevant conditions. *Soft Matter* **2014**, *10*, 175−186.

(20) Kim, K.; Choi, S. Q.; Zasadzinski, J. A.; Squires, T. M. Interfacial microrheology of DPPC monolayers at the air−water interface. *Soft Matter* **2011**, *7*, 7782−7789.

(21) Choi, S.; Steltenkamp, S.; Zasadzinski, J. A.; Squires, T. M. Active microrheology and simultaneous visualization of sheared phospholipid monolayers. *Nat. Commun.* **2011**, *2*, No. 312.

(22) Pieta, P.; Mirza, J.; Lipkowski, J. Direct visualization of the alamethicin pore formed in a planar phospholipid matrix. *Proc. Natl. Acad. Sci. U.S.A.* **2012**, *109*, 21223−21227.

(23) Forbrig, E.; Staffa, J. K.; Salewski, J.; Mroginski, M. A.; Hildebrandt, P.; Kozuch, J. Monitoring the orientational changes of Alamethicin during incorporation into bilayer lipid membranes. *Langmuir* **2018**, *34*, 2373−2385.

(24) Fontaine, P.; Ciatto, G.; Aubert, N.; Goldmann, M. Soft interfaces and resonant investigation on undulator source: a surface X-ray scattering beamline to study organic molecular films at the SOLEIL synchrotron. *Sci. Adv. Mater.* **2014**, *6*, 2312−2316.

(25) Pignat, J.; Cantin, S.; Liu, R. C. W.; Goldmann, M.; Fontaine, P.; Daillant, J.; Perrot, F. pH-dependent kinetics of MgCl 2 adsorption under a fatty-acid Langmuir film. *Eur. Phys. J. E* **2006**, *20*, 387−394.

(26) Evans, R. W.; Williams, M. A.; Tinoco, J. Surface viscosities of phospholipids alone and with cholesterol in monolayers at the air−water interface. *Lipids* **1980**, *15*, 524−533.

(27) Spaar, A.; Münster, C.; Salditt, T. Conformation of peptides in lipid membranes studied by X-ray grazing incidence scattering. *Biophys. J.* **2004**, *87*, 396−407.

(28) Majumdar, S.; Krishnaswamy, R.; Sood, A. K. Shear banding in a yield stress bearing Langmuir monolayer. *Soft Matter* **2011**, *7*, 7805−7812.

(29) Majumdar, S.; Sood, A. K. Statistical properties of entropy-consuming fluctuations in jammed states of laponite suspensions: Fluctuation relations and generalized Gumbel distribution. *Phys. Rev. E* **2012**, *85*, No. 041404.

(30) Sanyal, M. K.; Sinha, S. K.; Huang, K. G.; Ocko, B. M. X-ray-scattering study of capillary-wave fluctuations at a liquid surface. *Phys. Rev. Lett.* **1991**, *66*, 628−631.

(31) Guzmán, E.; Tajuelo, J.; Pastor, J. M.; Rubio, M. Á.; Ortega, F.; Rubio, R. G. Shear rheology of fluid interfaces: Closing the gap between macro-and micro-rheology. *Curr. Opin. Colloid Interface Sci.* **2018**, *37*, 33−48.

(32) Sánchez-Puga, P.; Tajuelo, J.; Pastor, J. M.; Rubio, M. A. Dynamic Measurements with the Bicone Interfacial Shear Rheometer: Numerical Bench-Marking of Flow Field-Based Data Processing. *Colloids Interfaces* **2018**, *2*, 69.

(33) Renggli, D.; Alicke, A.; Ewoldt, R. H.; Vermant, J. Operating windows for oscillatory interfacial shear rheology. *J. Rheol.* **2020**, *64*, 141−160.

https://dx.doi.org/10.1021/acsomega.0c01261
ACS Omega 2020, 5, 14555−14563